Gravitational radiation from cosmic strings

B. Allen*
Department of Physics, University of Wisconsin—Milwaukee, P.O. Box 413, Milwaukee, Wisconsin 53201

E. P. S. Shellard†
Department of Applied Mathematics and Theoretical Physics, Silver Street, Cambridge CB3 9EW, England
(Received 13 September 1991)

A cosmic-string network in an expanding universe evolves by losing energy to loops which in turn oscillate and emit gravitational radiation. The power radiated at a frequency corresponding to the nth fundamental mode of oscillation of the loop is characterized by a dimensionless constant P_n, with the total power radiated being proportional to $\gamma = \sum P_n$. Previously, these constants were estimated by analytic or numerical analysis in idealized situations, generally for simple loop shapes. Here, we determine these constants more realistically, for loops produced in a numerical simulation of the cosmic-string network. The resulting numerical values of the P_n appear to show a linear dependence on loop size, indicating that small-scale structure on the loops is very important in determining the overall radiation power. Long-string radiation is also studied, confirming this conclusion. The power radiated by a horizon-length string increases with time, because in the current simulations the small-scale structure on the string does not yet scale relative to the horizon length. With an appropriate extrapolation one can conclude that gravitational radiation from the long-string network will provide a significant energy-loss mechanism and may occur at a rate roughly comparable to energy loss due to loop formation.

PACS number(s): 98.80.Bp, 04.30.+x

I. INTRODUCTION

It is thought that the universe underwent several phase transitions as it expanded and cooled. In many unified theories, which describe the behavior of matter at very high energies, phase transitions of this type can lead to the formation of one-dimensional linear objects, known as cosmic strings [1–3]. These strings may be thought of as topologically trapped vortex lines; for the cases of cosmological interest these strings always form in closed loops or essentially infinite strings, and are primarily characterized by their mass per unit length μ. At the time of the phase transition, causality ensures that string segments formed in different causally disconnected regions of space are completely uncorrelated. Because of this, on length scales larger than the Hubble radius, strings are described by a random walk in three-dimensional space. For statistical reasons, with U(1) strings it turns out that $\approx 80\%$ of these random walks have infinite length; the remaining $\approx 20\%$ have finite length.

The time-evolution behavior of the resulting cosmic-string network has been extensively studied for about a decade. In the last four years, substantial progress has been made in understanding this behavior, primarily through the use of numerical simulations of the string network [4–6]. The network consists of long strings and loops, which are characterized respectively, as being longer or shorter than the horizon length. The numerical simulations have shown that the energy density in long strings is a small constant fraction of order $G\mu$ of the total cosmological energy density, where G is Newton's gravitational constant. This is referred to in the literature as the "scaling solution." If one lets t denote the proper time measured from the big bang by an observer at rest with respect to the cosmological fluid, this means that the energy density of long strings is $\rho = A\mu/t^2$. The dimensionless parameter A has been determined by the numerical simulations to have a value in the range 10–20 in the radiation-dominated era: our own numerical work [6] finds $A = 16 \pm 4$.

As the universe expands, the long strings continually cut off small loops, which oscillate and gradually convert their energy into gravitational radiation. This production of energy in the form of gravitational radiation is the main topic of this paper; we estimate the energy radiated by both the loops and by the long strings. The long-string network appears to have considerable substructure with many kinks and traveling waves, and analytic estimates have suggested that if certain assumptions hold, one might expect to find between 10^4 and 10^6 kinks per Hubble radius on the long string [7–9]. (Formally, a kink is a velocity discontinuity on the infinite string which resulted from an intercommutation. Such kinks travel at the speed of light, and slowly decay in amplitude.)

The gravitational radiation produced by the cosmic-string network has in the past been determined by a combination of analytic estimates and numerical work. The first work that considered the emission of gravitational

*Electronic address: ballen@dirac.phys.uwm.edu.
†Electronic address: epss@damtp.cambridge.ac.uk.

waves by cosmic-string loops was that of Vilenkin [10]. This early paper was a simplified order-of-magnitude calculation, and assumed that the dimensionless parameter $\gamma = \sum P_n$ characterizing the rate of emission was of order unity. Later, in a more detailed calculation, Turok [11] considered gravitational-wave emission from a two-parameter family of "looplike" strings which were artificially fixed at the two ends, and found γ in the range from 0.15 to 8. A year later, Vachaspati and Vilenkin [12] considered for the first time a realistic two-parameter family of cosmic-string loops, and found numerically that for these trajectories, $\gamma > 50$. This work was verified analytically and extended by Burden [13] who examined a three-parameter family of loops, again obtaining $\gamma > 50$. Two years later, Garfinkle and Vachaspati [14] considered a one-parameter family of "kinky" loops, containing velocity and direction discontinuities. They found values for γ in the range $\gamma > 45$. The most interesting work, and the most closely related to our own, was that done three years later by Scherrer, Quashnock, Spergel, and Press [15]. That work uses a numerical method that "evolves" the cosmic-string loops exactly in flat space, without introducing any errors at the intercommutations. This is the only work in which the back reaction (loop energy loss into gravitational radiation) is taken into account. The loops are allowed to fragment repeatedly until they reach a non-self-intersecting state, and the resulting family of loops was then studied in great detail. Starting from two rather different sets of initial conditions, the final sets of daughter loops were shown to have essentially identical distributions of γ, with more than half the non-self-intersecting loops having values of γ in the range from 40 to 60. The mean value found was $\gamma = 62$. The most recent work on the subject concerns infinite strings. Hindmarsh [9] analytically considers the gravitational radiation emitted by linear perturbations (structure) on an infinite straight string, and Quashnock and Spergel [16] numerically examined the back reaction effects due to kinks, obtaining a kink lifetime of order $l/(50G\mu)$ where l is the mean interkink distance.

This paper is intended to provide a step beyond these studies by examining gravitational radiation directly from the long-string network and from the loops it creates, in an expanding universe. The principal uncertainties in this work may be easily described. Because the *size* distribution of the loops produced by the current simulations do not appear to scale [6], we have to regard the *size* distribution obtained with some caution. Most loops are either created at a size within an order of magnitude of the minimum loop cutoff set in the simulation or else fragment down to these scales. In principle, however,the rate of gravitational-wave emission from some given loop does not depend upon the size of that loop, but only upon its shape. To state this more precisely: if loop A can be transformed into loop B by uniformly scaling its size, without changing the velocity of the string, then loops A and B radiate at the same rate. (We call two such loops *scale equivalent.*) Our results show that the energy radiation rate *does* depend upon the loop size. Thus the large loops produced in our simulation are *not* scale equivalent to the small loops. In fact our results suggest that the main mechanism by which the loops radiate gravitational radiation is via the oscillations associated with the small-scale bumps and kinks along the string. It appears that, in a first approximation, the energy radiated by loops is proportional to their length, indicating that all of the loops contain small-scale structure of fixed physical length.

The simulation incorporates a lower cutoff in the size of loops. This forbids any intercommutations which would result in the formation of a loop containing less than some given number of points (of order thirty). This artificial cutoff is required for practical considerations, because the evolution algorithms that we use require that the loops have at least a certain number of points. Consequently, the loops have substructure (short-length-scale convolutions) that would tend to be cut off the loops if our algorithms did not require an artificial cutoff. Thus, if the loops in our simulation do differ in shape from those that one might expect in the real world, they probably differ because they have too much substructure. Such substructure might be expected to enhance the total radiated energy, and consequently our energy-loss rates are probably reasonable upper bounds on the true values.

In the case of the long strings, the principal uncertainty is the mechanism by which structure forms on the long strings, and the mechanism by which this structure begins to scale. The numerical simulations do not have enough dynamic range in time to be able to see the scaling of structure on the long strings, and thus we are forced to make certain assumptions about these mechanisms in order to determine the rate at which gravitational radiation is emitted by the long strings. It is important to distinguish this continuing evolution of small-scale structure from the "scaling" behavior of the large-scale properties of the long-string network, about which there is considerable confidence. The evidence observed for this latter scaling includes the stability of the relative long-string energy density ($\rho_\infty t^2$), consistency with the long-string intercommuting rate, and the scaling of the long-string substructure energy per correlation length (even when the gravitational radiation spectrum has not begun to scale) [4–6].

A brief outline of the paper is as follows. In Sec. II, we examine the gravitational-wave emission by a spatially bounded source, and obtain a formula for this quantity in terms of the Fourier transform of the transverse spatial components of the source stress-energy tensor. In Sec. III, this formula is used to calculate the rate of gravitational-wave emission by an oscillating loop of cosmic string, and the radiated energy is expressed in terms of a pair of one-dimensional Fourier transforms of functions associated with the left- and right-moving components of the string. An essentially identical formula has also been obtained by Burden [13], and by other authors. In Sec. IV, a numerical algorithm to perform these computations is described, based on fast Fourier transform (FFT) techniques. In Sec. V, a series of numerical tests is described, based primarily on the differential and total emission from a planar loop of cosmic string, and from a kinky (Garfinke and Vachaspati) loop. These tests provide a nice demonstration of the various techniques.

Section VI presents the results for the gravitational-wave emission by cosmic-string loops. Section VII contains the corresponding results for long strings. This is followed by a short concluding Sec. VIII, which compares the relative magnitudes of the different energy-loss mechanisms for the cosmic-string network.

Note that within this paper, Newton's gravitational constant is denoted by G, and the speed of light by c. In most places, we set $c=1$, however in certain key formulas, the speed of light is included explicitly.

II. GRAVITATIONAL-WAVE EMISSION BY A BOUNDED SOURCE

The starting point of this work is a standard formula (Weinberg, [17]) which expresses the energy flux in gravitational waves emitted by an isolated radiating object with stress-energy tensor $T^{ab}(t,\mathbf{x})$. The metric perturbations induced by the gravitational waves are assumed to be small enough so that the space-time remains effectively flat; thus the effects of back reaction are neglected.

Far away from the isolated source, the power $d\dot{E}$ emitted per unit solid angle $d\Omega$ in the direction $\hat{\mathbf{\Omega}}$ at angular frequency ω in gravitational waves is given by

$$\frac{d\dot{E}}{d\Omega}=\frac{G\omega^2}{\pi c^5}[\tau^*_{ab}(\omega\hat{\mathbf{\Omega}})\tau^{ab}(\omega\hat{\mathbf{\Omega}})-\tfrac{1}{2}|\tau^a{}_a(\omega\hat{\mathbf{\Omega}})|^2] . \quad (2.1)$$

The spatial direction vector $\hat{\mathbf{\Omega}}$ has unit length $\hat{\mathbf{\Omega}}\cdot\hat{\mathbf{\Omega}}=1$, and τ_{ab} is the Fourier transform of the stress-energy tensor, defined by

$$\tau^{ab}(\mathbf{k})=\lim_{T\to\infty}\frac{1}{2T}\int_{-T}^{T}dt\int d^3\mathbf{x}\,e^{i(|\mathbf{k}|t-\mathbf{k}\cdot\mathbf{x})}T^{ab}(t,\mathbf{x}) . \quad (2.2)$$

The spatial part of the Fourier-transform integral (2.2) converges because we assume that the source is isolated, so that the stress-energy tensor vanishes outside a large sphere $|\mathbf{x}|^2=R^2$. On the other hand, the time part of the Fourier transform is expressed as an infinite-time limit, enabling us to consider a source that does not "turn off" at early or late times. In our case, since the string loops move periodically in time, losing only a tiny fraction (of order $G\mu$) of their energy in a single oscillation, the value of the time integral may be obtained by evaluating it over a single oscillation period of the string loop.

This formula may be simplified algebraically if one introduces a basis of four-vectors, $k^a=(1,\hat{\mathbf{\Omega}})/\sqrt{2}$, $l^a=(-1,\hat{\mathbf{\Omega}})/\sqrt{2}$, $v^a=(0,\hat{\mathbf{v}})$, and $w^a=(0,\hat{\mathbf{w}})$ where the unit three-vectors $\hat{\mathbf{\Omega}}$, $\hat{\mathbf{v}}$, and $\hat{\mathbf{w}}$ form an orthonormal triad. The vectors k^a and l^a are null, and have inner product $k^a l_a=1$. All other dot products among different basis vectors are zero.

Because the vector fields k^a, l^a, w^a, and v^a form a basis, the Fourier transform of the (symmetric) stress-energy tensor can be expressed in terms of them:

$$\begin{aligned}\tau^{ab}(\omega\hat{\mathbf{\Omega}})=&c_1k^ak^b+c_2l^al^b+c_3v^av^b+c_4w^aw^b\\&+c_5k^{(a}l^{b)}+c_6k^{(a}v^{b)}+c_7k^{(a}w^{b)}\\&+c_8l^{(a}v^{b)}+c_9l^{(a}w^{b)}+c_{10}v^{(a}w^{b)} .\end{aligned} \quad (2.3)$$

In this formula, the ten coefficients c_i are functions of the vector $\omega\hat{\mathbf{\Omega}}$. Conservation of the stress-energy tensor $\nabla_a T^{ab}=0$ now implies that

$$0=k_a\tau^{ab}=c_2l^b+\frac{c_5}{2}k^b+\frac{c_8}{2}v^b+\frac{c_9}{2}w^b . \quad (2.4)$$

Thus one has $c_2=c_5=c_8=c_9=0$. Now one can easily compute the square and trace of τ^{ab}. One obtains

$$\tau^{ab}\tau^*_{ab}=|c_3|^2+|c_4|^2+\tfrac{1}{2}|c_{10}|^2 \text{ and } \tau^a{}_a=c_3+c_4 . \quad (2.5)$$

Thus, the quantity appearing in formula (2.1) for $d\dot{E}/d\Omega$ is

$$\tau^*_{ab}\tau^{ab}-\tfrac{1}{2}|\tau^a{}_a|^2=\tfrac{1}{2}(|c_3-c_4|^2+|c_{10}|^2) . \quad (2.6)$$

This simplification shows that (1) the radiated energy is positive definite, and (2) the only components of τ^{ab} which are needed to determine the energy in gravitational waves radiated in direction $\hat{\mathbf{\Omega}}$ are the spatial components in the two spatial directions ($\hat{\mathbf{v}}$ and $\hat{\mathbf{w}}$) transverse to $\hat{\mathbf{\Omega}}$.

$$\begin{aligned}\frac{d\dot{E}}{d\Omega}=\frac{G\omega^2}{2\pi c^5}(&|\tau_{ab}v^av^b-\tau_{ab}w^aw^b|^2\\&+|\tau_{ab}v^aw^b+\tau_{ab}w^av^b|^2) .\end{aligned} \quad (2.7)$$

We note that the invariance of this quantity under rotations of the pair of vectors v^a and w^b in the spatial plane orthogonal to $\hat{\mathbf{\Omega}}$ can be explicitly demonstrated by writing it in the form

$$\begin{aligned}\frac{d\dot{E}}{d\Omega}=\frac{G\omega^2}{4\pi c^5}[&|\tau_{ab}(v^a+iw^a)(v^b+iw^b)|^2\\&+|\tau_{ab}(v^a-iw^a)(v^b-iw^b)|^2] .\end{aligned} \quad (2.8)$$

Under a rotation by angle θ around the axis defined by $\hat{\mathbf{\Omega}}$, the vectors $\hat{\mathbf{v}}\pm i\hat{\mathbf{w}}$ are only modified by pure phase factors:

$$v^a+iw^a\to e^{-i\theta}(v^a+iw^a),\quad v^a-iw^a\to e^{i\theta}(v^a-iw^a) , \quad (2.9)$$

and the radiated energy is unchanged. The phase factors $e^{\pm 2i\theta}$ appear in (2.8) because energy is being carried off in the helicity ± 2 states of the gravitational field.

Formula (2.8), which is valid for flat space-time, can also be applied to loops of cosmic string in an expanding universe. This is because the loops of string are smaller than the horizon length. The loops do not "see" the large-scale curvature of the universe, and behave exactly as if they were radiating into flat space-time.

III. GRAVITATIONAL RADIATION FROM LOOPS OF STRING

In order to calculate $d\dot{E}/d\Omega$, a practical method is needed to compute the Fourier transform of the stress-

energy tensor, τ^{ab}. In this section, τ^{ab} is expressed in terms of one-dimensional Fourier transforms. In the next section, we show how these quantities may be computed from our cosmic-string simulation using fast Fourier transform (FFT) techniques.

In flat space-time, consider a loop of cosmic string of energy M. The trajectory of the string is described by functions $y^a(\sigma,t)=(t,\mathbf{y}(\sigma,t))$, where σ is a spacelike parameter along the string world sheet in the range $\sigma\in[0,L]$, and t is time. In terms of the right- and left-moving fields $\mathbf{a}$ and $\mathbf{b}$, the string trajectory is described by

$$\mathbf{y}(\sigma,t)=\tfrac{1}{2}[\mathbf{a}(\sigma-t)+\mathbf{b}(\sigma+t)] . \tag{3.1}$$

In many of the standard treatments of cosmic strings, it is assumed that the coordinates $(t,\mathbf{x})$ are those in which the center of mass of the string loop is at rest, so that the string loop has no net momentum or overall linear velocity. However, the string loops produced in the numerical simulation are not at rest with respect to the rest frame of the cosmological fluid; they do have a net momentum (which is redshifted away by the expansion). As a result, the right- and left-moving fields satisfy the pseudoperiodicity conditions:

$$\begin{aligned}\mathbf{a}(u+L)&=\mathbf{a}(u)-\mathbf{V}L ,\\ \mathbf{b}(u+L)&=\mathbf{b}(u)+\mathbf{V}L .\end{aligned} \tag{3.2}$$

For a given string loop, these equations are satisfied for given fixed values of L and $\mathbf{V}$, and for all values of u. The velocity $\mathbf{V}$ of the center of mass of the string loop is given by

$$\mathbf{V}=\frac{1}{L}\int_0^L d\sigma\dot{\mathbf{y}} . \tag{3.3}$$

The pseudoperiodic conditions (3.2) ensure that the two ends $\sigma=0$ and $\sigma=L$ of the string touch, so that the length of string forms a periodic loop at any time. In addition, the right- and left-moving fields satisfy the conditions

$$\begin{aligned}\mathbf{a}'(\sigma)\cdot\mathbf{a}'(\sigma)&=1 ,\\ \mathbf{b}'(\sigma)\cdot\mathbf{b}'(\sigma)&=1 ,\end{aligned} \tag{3.4}$$

which ensure that the gauge condition $\dot{\mathbf{y}}(\sigma,t)\cdot\mathbf{y}'(\sigma,t)=0$ is satisfied. Here a prime denotes $d/d\sigma$ and an overdot denotes d/dt; they are derivatives with respect to the spatial and temporal parameters on the world sheet.

The stress-energy tensor of a loop of cosmic string in flat space-time is given by

$$T^{ab}(t,\mathbf{x})=\mu\int_0^L d\sigma[\dot{y}^a(\sigma,t)\dot{y}^b(\sigma,t)-y'^a(\sigma,t)y'^b(\sigma,t)]\delta^3(\mathbf{x}-\mathbf{y}(\sigma,t)) . \tag{3.5}$$

The quantity that appears in the integrand above can be expressed in the form of a four-by-four matrix:

$$\dot{y}^a\dot{y}^b-y'^a y'^b=\begin{bmatrix}1 & \dot{y}_s\\ \dot{y}_r & \dot{y}_r\dot{y}_s-y'_r y'_s\end{bmatrix} , \tag{3.6}$$

where r and s run from 1 to 3 and denote the spatial indices of the three-vector $\mathbf{y}$. The total energy (kinetic plus potential) of the string is now easily obtained, as

$$M=-\int d^3x\, T^0{}_0=\mu\int_0^L d\sigma=\mu L . \tag{3.7}$$

Hence $L=M/\mu$ is the invariant length of the loop. [This is the invariant length in the center-of-mass rest frame, times $(1-\mathbf{V}^2)^{-1/2}$].

Because the functions $\mathbf{a}$ and $\mathbf{b}$ are pseudoperiodic with period L (3.2), one can show that the motion of the string loop is periodic in time, apart from the uniform linear motion of its center of mass. However the period is not L as one might imagine, but is $L/2$. This is because the string's position and velocity repeat with this period:

$$\begin{aligned}\mathbf{y}(\sigma+L/2,t+L/2)&=\mathbf{y}(\sigma,t)+\mathbf{V}L/2 ,\\ \dot{\mathbf{y}}(\sigma+L/2,t+L/2)&=\dot{\mathbf{y}}(\sigma,t) .\end{aligned} \tag{3.8}$$

Note that the value of σ corresponding to the "same" point on the string after one period (time $L/2$ later) is not the same as the value of σ that corresponded to that point at time t. Nevertheless, at any time the loop is covered exactly once by the parameter range $\sigma\in[0,L]$.

Because of the time periodicity of the loop motion, the stress tensor of the string loop satisfies $T^{ab}(t,\mathbf{x})=T^{ab}(t+L/2,\ \mathbf{x}+\mathbf{V}L/2)$. This means that the Fourier transform $\tau^{ab}(\mathbf{k})$ defined by (2.2) must vanish except when the length of $\mathbf{k}$ takes on certain preferred values. To see this, consider

$$\tau^{ab}(\mathbf{k})=\lim_{T\to\infty}\frac{1}{2T}\int_{-T}^{T}dt\int d^3\mathbf{x}\, e^{i(|\mathbf{k}|t-\mathbf{k}\cdot\mathbf{x})}T^{ab}(t,\mathbf{x}) . \tag{3.9}$$

Since the integral is over all space and time, we can displace the integration variables, obtaining

$$\tau^{ab}(\mathbf{k})=\lim_{T\to\infty}\frac{1}{2T}\int_{-T}^{T}dt\int d^3\mathbf{x}\, e^{i[|\mathbf{k}|(t+L/2)-\mathbf{k}\cdot(\mathbf{x}+\mathbf{V}L/2)]}T^{ab}(t+L/2,\ \mathbf{x}+\mathbf{V}L/2) . \tag{3.10}$$

The periodic property of the stress-energy tensor shows that this equals

$$\tau^{ab}(\mathbf{k})=e^{i(|\mathbf{k}|-\mathbf{k}\cdot\mathbf{V})L/2}\lim_{T\to\infty}\frac{1}{2T}\int_{-T}^{T}dt\int d^3\mathbf{x}\, e^{i(|\mathbf{k}|t-\mathbf{k}\cdot\mathbf{x})}T^{ab}(t,\mathbf{x}) . \tag{3.11}$$

We thus conclude that $\tau^{ab}(\mathbf{k})=e^{i(|\mathbf{k}|-\mathbf{k}\cdot\mathbf{V})L/2}\tau^{ab}(\mathbf{k})$. The wave vector $\mathbf{k}$ may be written $\mathbf{k}=\omega\hat{\mathbf{\Omega}}$ where $\omega>0$ and $\hat{\mathbf{\Omega}}$ is a unit spatial three-vector. It follows immediately that $\tau^{ab}(\omega\hat{\mathbf{\Omega}})=0$ unless $\omega=\omega_n=4\pi n/L(1-\hat{\mathbf{\Omega}}\cdot\mathbf{V})$ for $n=1,2,3,\ldots$ a non-negative integer. [Since formula (2.1) contains an overall factor of ω^2, the $n=0$ mode cannot radiate]. We refer to the remaining $n=1,2,3,\ldots$ values of ω as the emission-mode frequencies of the loop.

The frequency at which gravitational radiation is emitted by a particular mode of the loop (labeled by n) depends upon the angle between the direction of emission and the direction of the center-of-mass velocity of the loop. As one might expect, the gravitational radiation emitted in the forward directions (along the velocity $\mathbf{V}\cdot\hat{\mathbf{\Omega}}>0$) is blueshifted to higher frequencies, and the radiation emitted in the backwards direction ($\mathbf{V}\cdot\hat{\mathbf{\Omega}}<0$) is redshifted. Along directions perpendicular to the center-of-mass velocity of the loop ($\mathbf{V}\cdot\hat{\mathbf{\Omega}}=0$) there is no frequency shift at all.

The Fourier transform of the stress tensor may now be rewritten in terms of an integral over a single oscillation period. To do this, we break the long time period $t\in(-T,T)$ into $2N$ intervals of length $L/2$. This gives

$$\begin{aligned}\tau^{ab}(\omega_n\hat{\mathbf{\Omega}})&=\lim_{N\to\infty}\frac{1}{NL}\sum_{j=-N}^{N-1}\int_{jL/2}^{(j+1)L/2}dt\,e^{i\omega_n t}\int d^3x\,e^{-i\omega_n\hat{\mathbf{\Omega}}\cdot\mathbf{x}}T^{ab}(t,\mathbf{x})\\&=\lim_{N\to\infty}\frac{1}{NL}\sum_{j=-N}^{N-1}\int_0^{L/2}dt\int d^3x\,e^{i\omega_n[t+jL/2-\hat{\mathbf{\Omega}}\cdot(\mathbf{x}+\mathbf{V}jL/2)]}T^{ab}(t+jL/2,\ \mathbf{x}+\mathbf{V}jL/2)\\&=\lim_{N\to\infty}\frac{1}{NL}\sum_{j=-N}^{N-1}[e^{i\omega_n L(1-\hat{\mathbf{\Omega}}\cdot\mathbf{V})/2}]^j\int_0^{L/2}dt\int d^3x\,e^{i\omega_n(t-\hat{\mathbf{\Omega}}\cdot\mathbf{x})}T^{ab}(t,\mathbf{x})\\&=\frac{2}{L}\int_0^{L/2}dt\,e^{i\omega_n t}\int d^3x\,e^{-i\omega_n\hat{\mathbf{\Omega}}\cdot\mathbf{x}}T^{ab}(t,\mathbf{x})\ .\end{aligned}\tag{3.12}$$

The second line above is obtained by shifting the integration variables in space and time. The third line then follows because of the periodic transformation property of the stress tensor. In this third line, the quantity in square brackets is unity for any of the emission-mode frequencies ω_n, and hence the summand is independent of j, from which the final line is obtained.

If one now uses expression (3.5) for the stress tensor, one obtains

$$\tau^{ab}(\omega_n\hat{\mathbf{\Omega}})=\frac{2\mu}{L}\int_0^{L/2}dt\,e^{i\omega_n t}\int_0^L d\sigma\,e^{-i\omega_n\hat{\mathbf{\Omega}}\cdot\mathbf{y}(\sigma,t)}\begin{bmatrix}1 & \dot{y}_s\\ \dot{y}_r & \dot{y}_r\dot{y}_s-y_r'y_s'\end{bmatrix}\ .\tag{3.13}$$

If r and s denote spatial indices, one may then express this in terms of the right- and left-movers $\mathbf{a}$ and $\mathbf{b}$, obtaining

$$\tau_{rs}(\omega_n\hat{\mathbf{\Omega}})=\frac{-2\mu}{L}\int_0^{L/2}dt\,e^{i\omega_n t}\int_0^L d\sigma\,e^{-i(\omega_n/2)\hat{\mathbf{\Omega}}\cdot[\mathbf{a}(\sigma-t)+\mathbf{b}(\sigma+t)]}a'_{(r}(\sigma-t)b'_{s)}(\sigma+t)\ ,\tag{3.14}$$

where the symmetrization symbol is $a'_{(r}b'_{s)}=(a'_rb'_s+b'_ra'_s)/2$. As earlier, the subscripts r and s denote the spatial components of $\mathbf{a}'$ and $\mathbf{b}'$

This integral may be reduced to the product of a pair of one-dimensional integrals, by introducing a set of null coordinates u and v.

$$u=\sigma-t,\quad v=\sigma+t\ .\tag{3.15}$$

The measures in the two coordinates systems are related by $du\,dv=2\,d\sigma\,dt$. The region of integration in the (u,v) plane is shown in Fig. 1; it consists of three regions labeled $R1$, $R2$, and $R3$ which taken together correspond to the rectangle $t\in[0,L/2]$ and $\sigma\in[0,L]$.

$$\tau_{rs}(\omega_n\hat{\mathbf{\Omega}})=\frac{-\mu}{L}\int\int_{R1\cup R2\cup R3}du\,dv\,I(u,v)\ .\tag{3.16}$$

The integrand is the function

$$I(u,v)=e^{i\omega_n(v-u)/2}e^{-i\omega_n\hat{\mathbf{\Omega}}\cdot[\mathbf{a}(u)+\mathbf{b}(v)]/2}a'_{(r}(u)b'_{s)}(v)\ .\tag{3.17}$$

It is now possible to show that $I(u+L,\ v)=I(u,v)$, so that the integrand takes on identical values in regions $R1$ and $R1'$ of Fig. 1. This is because $a'(u+L)=a'(u)$ is periodic, and because

$$\begin{aligned}e^{i\omega_n(v-u-L)/2-i\omega_n\hat{\mathbf{\Omega}}\cdot[\mathbf{a}(u+L)+\mathbf{b}(v)]/2}&=e^{i\omega_n(v-u)/2-i\omega_n\hat{\mathbf{\Omega}}\cdot[\mathbf{a}(u)+\mathbf{b}(v)]/2}e^{-i\omega_nL(1-\hat{\mathbf{\Omega}}\cdot\mathbf{V})/2}\\&=e^{i\omega_n(v-u)/2-i\omega_n\hat{\mathbf{\Omega}}\cdot[\mathbf{a}(u)+\mathbf{b}(v)]/2}\ .\end{aligned}\tag{3.18}$$

By a similar argument, one can show that $I(u,\ v+L)=I(u,v)$ and hence that the integral over region $R2$ is the same as the integral over the region $R2'$. One thus obtains an integral over the square region $u,v\in[0,L]$.

$$\tau_{rs}(\omega_n\hat{\Omega})=\frac{-\mu}{L}\int_0^L du\int_0^L dv\, e^{i\omega_n(v-u)/2}e^{-i\omega_n\hat{\Omega}\cdot[\mathbf{a}(u)+\mathbf{b}(v)]/2}a'_{(r}(u)b'_{s)}(v)$$
$$=\frac{-\mu}{L}\left[\frac{L}{2\pi}\right]^2 A_{(r}(\omega_n\hat{\Omega})B_{s)}(\omega_n\hat{\Omega})\ , \tag{3.19}$$

where the quantities A_r and B_r are defined by the following Fourier transforms:

$$\mathbf{A}(\omega_n\hat{\Omega})=\frac{2\pi}{L}\int_0^L e^{-i(\omega_n/2)[u+\hat{\Omega}\cdot\mathbf{a}(u)]}\mathbf{a}'(u)du\ ,$$
$$\mathbf{B}(\omega_n\hat{\Omega})=\frac{2\pi}{L}\int_0^L e^{i(\omega_n/2)[v-\hat{\Omega}\cdot\mathbf{b}(v)]}\mathbf{b}'(v)dv\ . \tag{3.20}$$

The problem of calculating the energy radiated by a loop of cosmic string is thus reduced to the problem of finding the spatial components of a pair of one-dimensional integral transforms. An essentially identical formula occurs in Eq. (7) of Burden [13], although in that work it is assumed that the center of mass of the cosmic-string loop is at rest.

There is still some additional complication involved in computing the functions **A** and **B**. This arises because the right- and left-moving vector fields **a** and **b** are not stored directly in the simulation (however their derivatives **a'** and **b'** are readily available). Moreover, the forms of **A** and **B** are not yet Fourier transforms that can be evaluated by (for example) an FFT algorithm. To put the **A** integral (for example) into an easily computable form, one changes to a new variable

$$x=\frac{2\pi}{L(1-\mathbf{V}\cdot\hat{\Omega})}\{u+\hat{\Omega}\cdot[\mathbf{a}(u)-\mathbf{a}(0)]\}$$

with

$$dx=\frac{2\pi}{L(1-\mathbf{V}\cdot\hat{\Omega})}[1+\hat{\Omega}\cdot\mathbf{a}'(u)]du\ .$$

Note that because both $\hat{\Omega}$ and **a'** have unit length, the quantity $[1+\hat{\Omega}\cdot\mathbf{a}'(u)]$ lies in the range [0,2]. Consequently, x is a monotonically increasing function of u. Since **a** is a pseudoperiodic function, the range $u\in[0,L]$ corresponds to a range of the new variable $x\in[0,2\pi]$. One obtains (modulo a pure phase factor $e^{i\delta}$ which cancels out of $d\dot{E}/d\Omega$)

$$\mathbf{A}(\omega_n\hat{\Omega})=(1-\mathbf{V}\cdot\hat{\Omega})\int_0^{2\pi}dx\, e^{-inx}\boldsymbol{\alpha}(x)$$
$$\text{with } \boldsymbol{\alpha}(x)=\frac{\mathbf{a}'(u)}{1+\hat{\Omega}\cdot\mathbf{a}'(u)}\ . \tag{3.21}$$

Note that in this expression, the derivatives $\mathbf{a}'(u)$ denote derivatives with respect to the original parameter u of the string. They do *not* denote derivatives with respect to the new parameter x along the string. Thus, the vector field $\mathbf{a}'(u)$ is still *unit length* (3.4). The corresponding expression for **B** is

$$\mathbf{B}(\omega_n\hat{\Omega})=(1-\hat{\mathbf{V}}\cdot\hat{\Omega})\int_0^{2\pi}dx\, e^{inx}\boldsymbol{\beta}(x)$$
$$\text{with } \boldsymbol{\beta}(x)=\frac{\mathbf{b}'(u)}{1-\hat{\Omega}\cdot\mathbf{b}'(u)}\ , \tag{3.22}$$

where once again, the vector field $\mathbf{b}'(u)$ has unit length. Each component of the vectors **A** and **B** has now been expressed as a Fourier transform, of $\boldsymbol{\alpha}$ and $\boldsymbol{\beta}$, respectively.

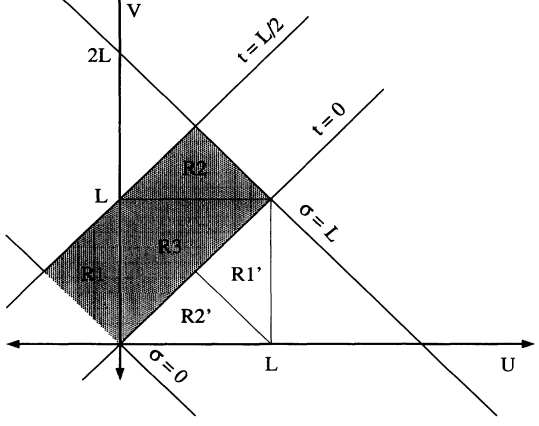

FIG. 1. The region over the (u,v) plane used to evaluate the integral in Eq. (3.16). The integrand (3.15) is the same in regions $R1$ and $R1'$ and in regions $R2$ and $R2'$. Hence the integral over the shaded region equals the integral over the $L\times L$ square.

IV. NUMERICAL COMPUTATION OF THE FOURIER TRANSFORM OF THE STRESS-ENERGY TENSOR

To compute these quantities numerically, the following procedure is used. Here, we illustrate the method for **A**; the method for **B** is similar. We label the N segments making up the string loop by $i=1,\ldots,N$. At each of these segments, the quantities $\mathbf{a}'_i$, $\mathbf{b}'_i$ and du_i are known (these quantities are fundamental variables that our numerical simulation evolves at each time step). The quantity du_i represents the "Lorentz-uncontracted length" of the ith segment; the total energy of the loop is

$$\mu L=\mu\sum_{i=1}^{N}du_i\ . \tag{4.1}$$

For a given, predetermined choice of direction $\hat{\Omega}$, one defines the quantities

$$\Delta x_i=(1+\hat{\Omega}\cdot\mathbf{a}'_i)du_i,\quad i=1,\ldots,N\ . \tag{4.2}$$

The sum of these small increments [times $2\pi/L(1-\mathbf{V}\cdot\hat{\Omega})$] defines the quantities x_i, which correspond to the variable of integration x defined immediately before Eq. (3.21):

$$x_i=\sum_{j=1}^{i}\Delta x_j,\quad i=1,\ldots,N\ . \tag{4.3}$$

Since the function $a(u)$ is periodic, $\sum_{i=1}^{N}\mathbf{a}'_i du_i=0$, and hence $x_N=L$.

The integrand for the Fourier transform is a function $\boldsymbol{\alpha}(x)$, which is now discretely defined by three sets of N pairs of points $(x_i, \hat{\mathbf{x}}\cdot\boldsymbol{\alpha}_i)$, $(x_i, \hat{\mathbf{y}}\cdot\boldsymbol{\alpha}_i)$, and $(x_i, \hat{\mathbf{z}}\cdot\boldsymbol{\alpha}_i)$, where $\boldsymbol{\alpha}_i = \boldsymbol{\alpha}(x_i)$,

$$\boldsymbol{\alpha}_i = \mathbf{a}_i' du_i/\Delta x_i, \quad i = 1, \ldots, N \ . \tag{4.4}$$

If the x_i were equally spaced (i.e., $\Delta x_i = \text{constant}$) and N were a power of 2, one could simply apply standard fast Fourier transform (FFT) techniques three times. However the values of x_i are not in general evenly spaced. In order to use an FFT to evaluate $\mathbf{A}$, we need to estimate (interpolate) the values of the function $\boldsymbol{\alpha}(x)$ on an evenly spaced grid of x's. We will denote this evenly spaced grid of x's by $\bar{x}_i$ where $i = 1, \ldots, M$. For optimal efficiency, the number M of equally spaced points should be a power of 2.

We first choose $M = 2^s 2^p$ where s is the smallest integer not less than $\log_2 N$, and p is an integer between 3 and 13 which increases the number of interpolated points to prevent anti-aliasing in the FFT. The evenly spaced points are then

$$\bar{x}_i = \frac{i}{M} x_N, \quad i = 1, \ldots, M \ . \tag{4.5}$$

The values of the function $\boldsymbol{\alpha}(\bar{x}_i)$ are determined at these evenly spaced points in a very simple way. Any given point lies on some particular segment, i.e., $x_r < \bar{x}_i < x_{r+1}$. Here the integer r labels the particular segment of string; it lies in the range $1 \le r \le N$. The value of $\boldsymbol{\alpha}(\bar{x}_i)$ is then taken to be exactly the value of $\boldsymbol{\alpha}$ for that segment, i.e., $\boldsymbol{\alpha}(x_r)$. This method, which involves *no* interpolation, models the loop of string as being composed of exactly N straight segments, each of which has uniform velocity and a constant tangent vector. Hence the integrand of the FFT is piecewise constant. Many other interpolation methods, including polynomial interpolation, rational-function interpolation and cubic-spline interpolation were also tried, and were found to be about equally effective at preventing anti-aliasing; we chose the fastest method.

The function being Fourier transformed is defined by the pairs of points $(x_i, \boldsymbol{\alpha}_i)$. In regions where $\hat{\boldsymbol{\Omega}}\cdot\mathbf{a}'$ is very close to -1, the values of Δx_i are quite close to zero. For this reason, the successive x_i's are space very close together, and the values of $\boldsymbol{\alpha}_i$ are quite large. These smallest segments are those regions directed along line-of-sight $\hat{\boldsymbol{\Omega}}$ vector; these segments contribute large amounts of high-frequency energy to the Fourier transform of $\boldsymbol{\alpha}$, since over a small range of x the function $\boldsymbol{\alpha}(x)$ becomes large. If the number of points M used for the discrete FFT is too small to represent this highest frequency, then some of the energy that should end up at high frequencies gets shifted (or "aliased") to lower frequencies. The "piecewise-constant" interpolation method that we use has as its principle advantage that the points $\bar{x}_i$ tend to fall very infrequently onto those tiny segments where the successive x_i's are spaced very close together, and the values of $\boldsymbol{\alpha}_i$ are quite large. In production work, we increase p until every segment is landed on at least once (typically $M = 2^{s+p} \ge 2^{16}$). In the unlikely event that we do step onto one of these tiny segments, the value of the integrand is limited to a maximum value of $\pm M/16$; however, this limiting is invoked only very rarely. By increasing the inverse of the spacing interval until all segments are landed on, we ensure that the inverse of the spacing interval is greater than twice the Nyquist frequency of α. This is for statistical reasons: further increases in M do not change the fraction of points with any given value $\boldsymbol{\alpha}_i$. This proved to be an effective means of preventing anti-aliasing. In future work, it would be desirable to use analytic expressions for the energy radiated from string segments which have $\mathbf{a}'$ antiparallel to $\hat{\boldsymbol{\Omega}}$ or $\mathbf{b}'$ parallel to $\hat{\boldsymbol{\Omega}}$.

In the tests described in the next section, the value of p was kept very small ($p = 3$ or $p = 4$) to provide an especially stringent test of the algorithm. It was found that in the worst case, energy radiated in the plane of the loop, the number of frequency values n which were reliable was always at least $M/10$. Thus, by using large numbers of interpolating points, we were able to generate reliable values of P_n for $n \gg N$.

If we denote the discrete Fourier transform of the points $\alpha(\bar{x}_i)$ by $F[\alpha]_n$ and the corresponding Fourier transform for $\beta(\bar{x}_i)$ by $F[\beta]_n$ then one has

$$\frac{d\dot{E}_n}{d\Omega} = \frac{G\mu^2 c n^2 (1-\hat{\boldsymbol{\Omega}}\cdot\mathbf{V})^2}{4\pi^3}\{|F[\boldsymbol{\alpha}\cdot(\hat{\mathbf{v}}+i\hat{\mathbf{w}})]_n|^2|F[\boldsymbol{\beta}\cdot(\hat{\mathbf{v}}+i\hat{\mathbf{w}})]_{-n}|^2 + |F[\boldsymbol{\beta}\cdot(\hat{\mathbf{v}}+i\hat{\mathbf{w}})]_n|^2|F[\boldsymbol{\alpha}\cdot(\hat{\mathbf{v}}+i\hat{\mathbf{w}})]_{-n}|^2\} \ . \tag{4.6}$$

We define a set of dimensionless constants P_n by the equation

$$\dot{E}_n = G\mu^2 c P_n = \int \frac{d\dot{E}_n}{d\Omega} d\Omega \ . \tag{4.7}$$

This formula gives the power radiated per unit solid angle at the frequency ω_n. The dimensionless constants characterizing the radiation rate are

$$P_n = \frac{n^2(1-\hat{\boldsymbol{\Omega}}\cdot\mathbf{V})^2}{4\pi^3}\int\{|F[\boldsymbol{\alpha}\cdot(\hat{\mathbf{v}}+i\hat{\mathbf{w}})]_n|^2|F[\boldsymbol{\beta}\cdot(\hat{\mathbf{v}}+i\hat{\mathbf{w}})]_{-n}|^2 + |F[\boldsymbol{\beta}\cdot(\hat{\mathbf{v}}+i\hat{\mathbf{w}})]_n|^2|F[\boldsymbol{\alpha}\cdot(\hat{\mathbf{v}}+i\hat{\mathbf{w}})]_{-n}|^2\} d\Omega \ . \tag{4.8}$$

The reader will note that all reference to the length L has disappeared from this expression, since $\boldsymbol{\alpha}$, $\boldsymbol{\beta}$, and their corresponding FFT's are dimensionless. This is a direct consequence of the "scale independence" of the P_n's, discussed near the end of the Introduction, in Sec. I.

In order to determine P_n it is necessary to integrate $d\dot{E}_n/d\Omega$ over all directions on a two-sphere. The only way to do this integral for a general string network is by

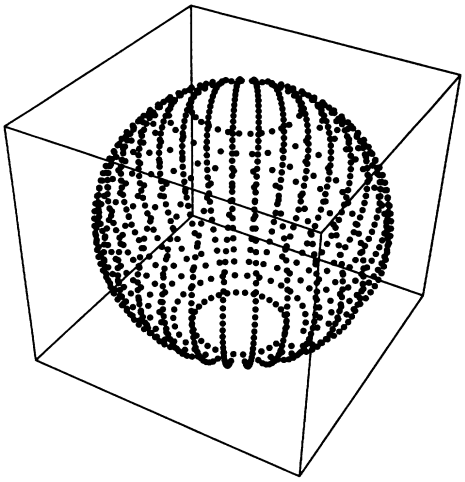

FIG. 2. In order to integrate over the sphere, a set of points is chosen at which to determine $dP_n/d\Omega$. This set of points is obtained by Cantor interpolation; the set is shown for five levels of interpolation, corresponding to $(2^5-1)^2$ points.

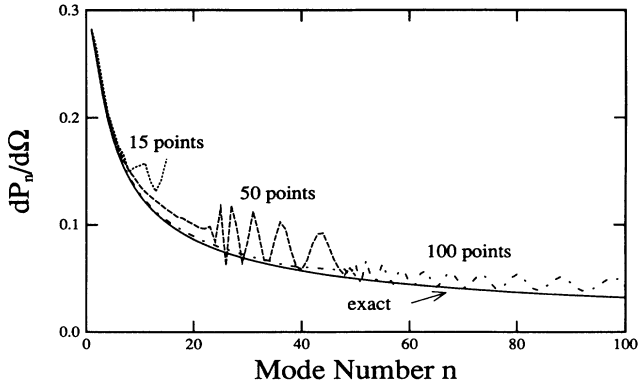

FIG. 3. The calculated gravitational emission $dP_n/d\Omega$ from an exact planar circular loop is shown in the equatorial plane $\theta=\pi/2$ as a solid line. The remaining three curves show the numerical algorithm of this paper applied to discrete circular loops composed of 15, 50, and 100 points. The radiation in the equatorial plane falls off very slowly with increasing n, and is the most difficult test of a numerical method.

choosing directions on the two-sphere, and then sampling $d\dot{E}_n/d\Omega$ at those points. The sequence of points that we use is shown in Fig. 2; the results for the string network are (quite sensibly) independent of the set of directions that are used, because the thousands of loops produced in a typical run of our numerical simulation are randomly oriented.

V. NUMERICAL TESTS

In order to test the numerical methods, the code to calculate $d\dot{E}_n/d\Omega$ was used to analyze a plane circular loop. In this case the answer was obtained analytically by Vilenkin and Vachaspati [12], and then later reproduced by Burden [13]. They analyzed the case of an ideal plane circular loop (here called a "smooth loop"). Most of the energy is radiated near $\theta=\pi/2$ where θ is the equatorial angle measured from the axis of symmetry of the loop. In this direction, the exact result for the "smooth loop" is given by Eq. (2.16) of [12] as

$$dP_n/d\Omega|_{\theta=\pi/2}=\frac{\pi}{2}n^2[J_{n+1}(n)-J_{n-1}(n)]^4\ , \qquad (5.1)$$

where J_n is a Bessel function of order n. A more general formula [Eq. (2.15) of [12]] is also given for the energy radiated in an arbitrary direction θ. This exact result is shown for comparison purposes in Figs. 3 and 4.

In Fig. 3, the exact result for $dP_n/d\Omega$ in the direction $\theta=\pi/2$ is compared to the numerical results obtained for loops composed of $N=15$, 50, and 100 points. The "discrete loops" do not agree precisely with the exact result because they are composed of N straight kinks, and are not in any sense "smooth." For smaller angles $\theta<\pi/2$ which are not shown, these "discrete loops" are in much closer agreement with the exact "smooth loop" results.

In Fig. 4, the exact result for a "smooth loop" is compared to the numerical one for a "discrete loop" composed of 1000 points, for three different values of θ. For gravitational waves radiated in the directions $\theta=\pi/4$ and $\theta=3\pi/8$ the exact results are indistinguishable from the numerical ones. The only difference appears for $\theta=\pi/2$, where the numerical results for the "discrete loop" are seen to contain slightly more energy at high frequencies than the ideal "smooth loop." This is because the number of interpolating points is only a factor of 8 ($p=3$) greater than the number of loop points. Increasing the number of interpolating points M in this case reduces the excess emission and makes the numerical result indistinguishable from the exact one. In all of our production runs, we set p much larger than 3 to prevent these types of effects.

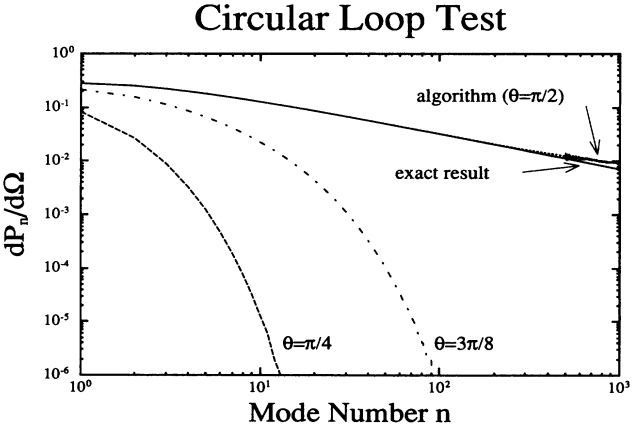

FIG. 4. Gravitational radiation from a circular loop, shown in three directions, $\theta=\pi/4$, $\theta=3\pi/8$, and $\theta=\pi/2$. This is compared to the result of the numerical algorithm for a discrete, 1000-point loop. For the first two values of θ, the exact result and the algorithm result cannot be distinguished on the graph. In the case of $\theta=\pi/2$ the exact result gives slightly less high-frequency energy. This is because the discrete loop contains small kinks which increase its emission at high frequencies.

The method of integration described at the end of Sec. IV was also tested using an ideal plane circular "smooth loop." In this case, the value of P_n (an integral over the two-sphere) reduces to a single integral over the equatorial angle θ. In order to provide a realistic test, this symmetry was not exploited. The resulting P_n are shown in Fig. 5, for loops containing 15, 50, 100, and 1000 points. For comparison purposes, Fig. 5 also shows the exact P_n, obtained by integrating the analytic differential formula of Vachaspati and Vilenkin. The resulting curves (numerical and analytic) are almost indistinguishable. In all cases, the resulting P_n are slightly larger than the exact values, leading us to conclude that our results for γ provide upper bounds to its value. This test demonstrates the accuracy of our methods in the continuum limit for a smooth loop.

We have also tested the algorithm on a family of loops possessing kinks. We used a particularly simple set of kinky-loop solutions for which γ was determined analytically by Garfinkle and Vachaspati ([14], first paper). The family of kinky loops is defined by

$$\begin{aligned}
\mathbf{a} &= \left[u - \frac{L}{4}\right]\mathbf{A}, \quad 0 \le u < \frac{L}{2}, \\
\mathbf{a} &= \left[\frac{3L}{4} - u\right]\mathbf{A}, \quad \frac{L}{2} \le u < L, \\
\mathbf{b} &= \left[v - \frac{L}{4}\right]\mathbf{B}, \quad 0 \le v < \frac{L}{2}, \\
\mathbf{b} &= \left[\frac{3L}{4} - v\right]\mathbf{B}, \quad \frac{L}{2} \le v < L,
\end{aligned} \tag{5.2}$$

where **A** and **B** are arbitrary unit vectors. The loops consist of four straight segments separated by four kinks; two kinks propagate in the opposite direction to the other two. In the special case with $\mathbf{A}\cdot\mathbf{B}=0$, the loop is planar and oscillates between being a square and a doubled line.

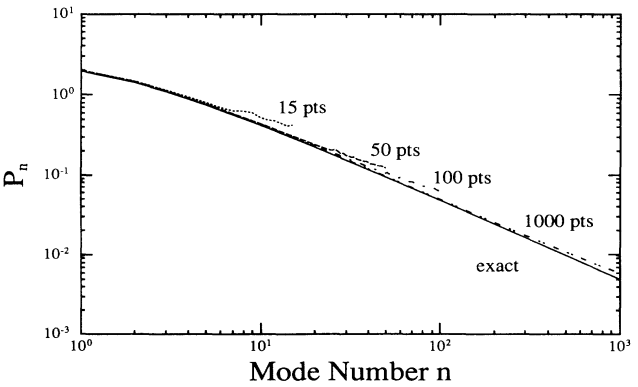

FIG. 5. The value of P_n for an ideal planar circular loop is shown by the solid lower line. The remaining three curves show the results obtained numerically for a discrete circular loop consisting of 15, 50, and 100 points, respectively. These results are obtained by numerically integrating $dP_n/d\Omega$ over the surface of a two-sphere. This is done by adding up the value of $dP_n/d\Omega$ at 916 points uniformly spaced over the surface of the sphere, as shown in Fig. 2.

The radiation rate for these solutions can be evaluated analytically, and is given in Eq. (3.9) of the first paper of Ref. [14]. In the special case where **A** and **B** are perpendicular the result is

$$\gamma = 64 \ln 2 \approx 45 . \tag{5.3}$$

These loops were created as initial conditions for the numerical code and used to test both the evolution and gravity-wave algorithms. As reported earlier, the evolution algorithm proved reliable for many thousands of time steps in an expanding universe, provided the number of points on a loop was above a threshold near $N > 20$. For a kinky 32-point loop, energy conservation was 98% and the other gauge constraint $< 1\%$ after 2000 time steps. In order to calculate the gravitational radiation rate we sampled $dP/d\Omega$ with the wave vector $\mathbf{k} = \omega_n \hat{\mathbf{\Omega}}$ pointing in random directions. For the perpendicular loop, we obtained a convergence of γ to within 5% of the result (5.3) for any sampling number beyond 64, and considerable improvement beyond this. For loops with $N = 32$ points and above, the value of γ was time independent even after thousands of time steps. This result demonstrates the correct operation of the gravitational-radiation algorithms. It also shows that for samples of many more than 100 randomly oriented loops containing kinks, an accurate value for the average of γ can be obtained by sampling in only one direction **k**.

VI. NUMERICAL RESULTS FOR LOOPS

The main interest is in the gravitational radiation during the epoch when the universe is radiation dominated. Our simulation is run until well after the time at which the energy density in the infinite strings begins to scale. The lower limit on loop size is set to 30 points, in the regime where the accuracy of the gravitational-radiation algorithms has been tested. The P_n are then determined for those loops whose length at that time is less than πL, where $L = 2t$ is the horizon length. To prevent antialiasing, the value of p, defined before Eq. (4.5), was increased to large values, corresponding to at least $2^{16} = 65\,536$ points per loop.

To see how the P_n depend upon the size of the loops, the loops are binned by energy. The equally logarithmically spaced bins are labeled by an integer $k = 0, 1, 2, \ldots$. A loop of energy μl is placed into bin k if its length l lies in the range $\pi L 2^{-k-1} \le l < \pi L 2^{-k}$, where L is the horizon length. The results are shown in Figs. 6(a)–6(c), which show the P_n for the different-sized loops at three different times. The corresponding values of

$$\gamma = \sum_n P_n \tag{6.1}$$

are shown in Fig. 6(d). The time in Figs. 6(a)–6(d) may be quickly determined from the ratio L/L_f of the horizon length L to the horizon length L_f when the simulation was started.

It can be readily seen that over more than three orders of magnitude in loop length, γ varies linearly with l. This seems to indicate that all of the loops contain small-

scale structure at a fixed physical length scale, and that the total energy being radiated from a loop therefore is some constant times the total length of the loop. In Fig. 6(d), the mean values of the emission rate and loop length at the three times are

$$(\langle\gamma\rangle,\langle l\rangle)=\begin{cases}(\langle\gamma\rangle=69.3,\langle l\rangle=0.528L_f)\\ \quad\text{when } L/L_f=8.97\ ,\\ (\langle\gamma\rangle=64.4,\langle l\rangle=0.455L_f)\\ \quad\text{when } L/L_f=32.87\ ,\\ (\langle\gamma\rangle=64.8,\langle l\rangle 0.459L_f)\\ \quad\text{when } L/L_f=61.23\ .\end{cases} \tag{6.2}$$

The mean values of γ are between 64 and 70 at all three times. Noting that our cutoffs prevent the loops from shedding at least some of their small-scale structure and further reducing their gravitational radiation rate, we obtain a fairly conservative upper bound of $\gamma\sim 65$, which is quite consistent with the results of Scherrer, Quashnock, Spergel, and Press [15].

We noted in the Introduction that, while the large-scale properties of the network are scaling in the simulation, the spectrum of substructure and the loop-production function were not. In a realistic scaling solution our expectation is the loops would be created and fragment to smaller sizes than permitted by the current numerical resolution. At least some loops, therefore, should possess excess substructure. Since we observe that the loop substructure is a significant source of gravitational radiation this will produce more gravitational radiation and therefore an upper bound for γ. We also do not introduce gravitational back reaction, so that small-scale structure that would be expected to be smoothed out on a time scale considerably shorter than the loop lifetime continues to radiate. During the latter stages of

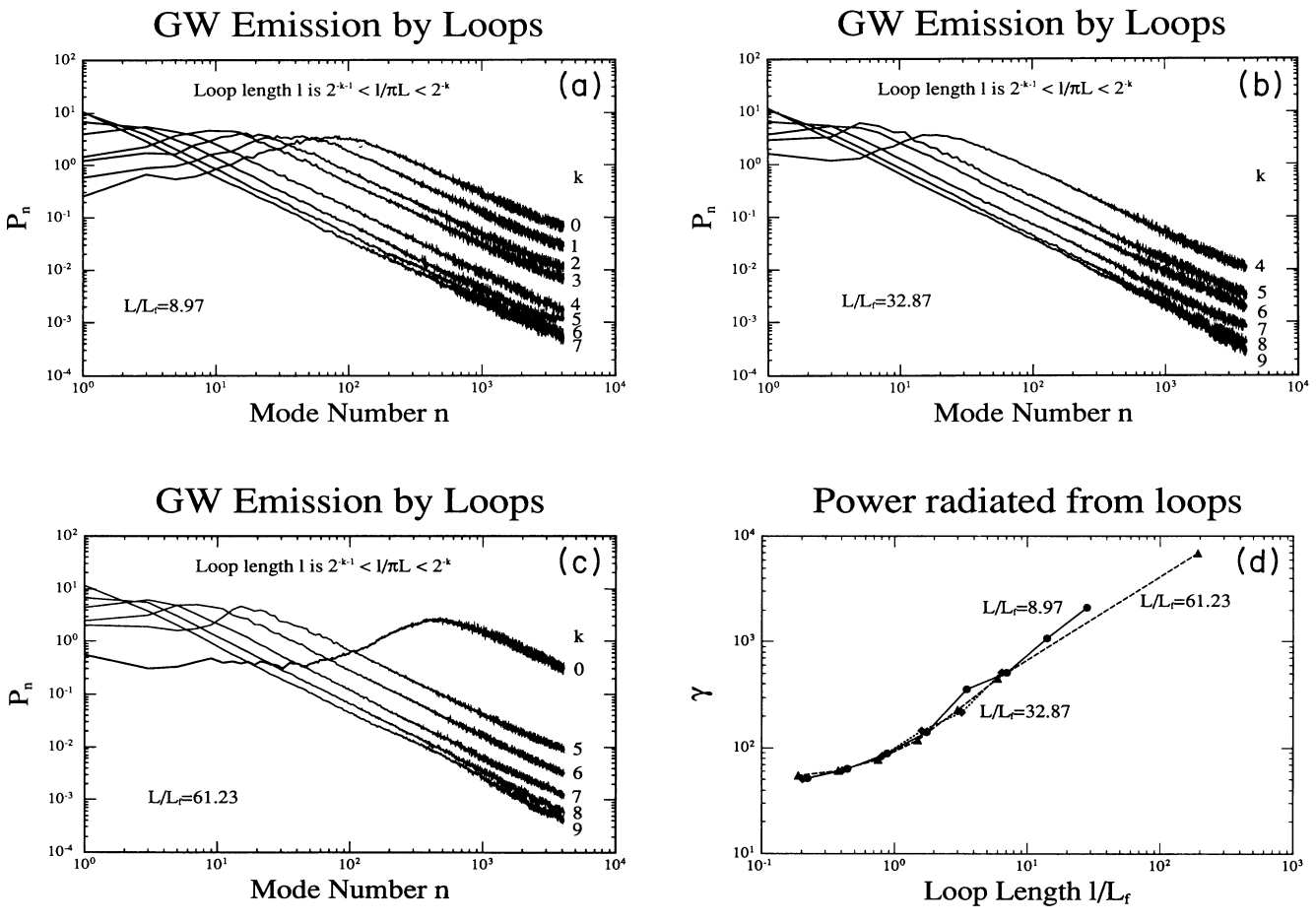

FIG. 6. The three graphs show P_n as a function of n, for loops whose invariant length l is less than π times the horizon length L. In graph (a), the horizon has expanded to 8.97 times its initial value L_f, in graph (b) to 32.87 times its initial value, and in graph (c) to 61.23 times its initial value. In each of the three graphs, the curves labeled by k correspond to loops with a different range of l. For curve k, the loop size l lies in the range $\pi L 2^{-k-1}\le l<\pi L 2^{-k}$. The P_n decrease with decreasing l. For large n, the P_n fall off at a rate between $n^{-1.2}$ and $n^{-1.4}$. The sum of these P_n determine γ, the total energy-loss rate from the loop. (d) This graph shows γ as a function of loop length for each of the three times in graphs (a), (b), and (c). This graph includes a small correction for the missing area under the large-n tail of the first three graphs. The mean values of γ and l/L_f at the early, intermediate, and late time, respectively, are given in Eq. (6.2). For a given loop size, the value of γ is independent of time, as one might hope.

loop decay, the lower harmonics would begin to predominate reducing the effective γ. Again, this would act to make our estimate an upper bound.

It is interesting to note the fairly good agreement with the flat-space results of Scherrer *et al.* [15], since the loop-production processes are so different. They study daughter loops produced by the fragmentation of a smooth convoluted parent loop in flat space whereas, in our case, we have fractal long strings with low coherent velocities which produce small loops directly in collapsing regions [6]. This appears to lend support to their claim that loops that are the end products of a fragmentation process will have properties independent of their earlier evolution. Although their results do not set a scale for the loops produced by a network in an expanding universe, they may well be relevant for their other properties.

VII. INFINITE STRINGS

In this section, we will obtain the spectrum of radiation emitted by the infinite strings. Because the infinite strings are not small relative to the horizon length, they feel the effects of the large-scale curvature of space-time, or in other words, the expansion of the universe. At present, there is no formalism available which gives the expanding-universe equivalent of Eq. (2.1), expressing the rate at which an isolated system radiates energy in gravitational waves. Thus, in this section, we *assume* that the flat-space formula (2.1) can be applied in curved space, and that it is correct for energy radiated in modes whose wavelength is significantly smaller than the horizon length.

In the case of small loops of cosmic string, the fundamental (lowest) frequency is set by the length L of the loop to be $\omega=4\pi c/L$. In the case of the infinite strings, we expect that on physical grounds the long strings will radiate only above a minimum frequency of order $\omega=4\pi c/L_h$, where L_h is the radius of the horizon (horizon length). This is for the following reasons. First, on length scales longer than L_h the infinite strings are not correlated, for reasons of causality. Second, for "wavelengths" longer than L_h, the energy carried in gravitational waves vanishes because the universe is not old enough for the waves to have had time to oscillate even once. Lastly, since the strings are created by a causal process, on long length scales they are necessarily isocurvature perturbations, and their energy must be compensated by a deficit in the surrounding cosmological fluid. Thus, on length scales larger than the horizon, the Fourier components of the stress-energy tensor are suppressed.

In this section, we assume that the universe is radiation dominated. The space-time metric is $ds^2=-dt^2+a^2(t)d\mathbf{x}^2$ with cosmological scale factor $a(t)=t^{1/2}$. Thus, $L_h=2t$ is the horizon length. The spatial section forms a three-torus, whose coordinate size is fixed, so that the range of the comoving coordinates $x,y,z\in[0,L_{\rm box}]$. Thus the volume at any time t is $V(t)=a^3(t)L_{\rm box}^3$. The energy density in infinite strings is given by $\rho_\infty=\mu A t^{-2}$ with $A\approx 16$. The simulation is started at the "formation time" t_f with an initial horizon length $L_f=2t_f$, and an initial correlation length on the infinite-string network given by $L_f/8$.

The gravitational radiation in the infinite strings can be characterized completely in terms of a set of dimensionless coefficients, C_n. These coefficients are analogous to the P_n for the loops. In particular, the value of C_n determines the rate of gravitational radiation at angular frequency

$$\omega_n=4\pi n/L_h\ , \tag{7.1}$$

where the mode index $n=1,2,\ldots$. The crucial difference is that the frequency of the mode n is determined entirely by the horizon length. In addition, as we will define them, the C_n's include the effects of *all* the infinite strings; they do not simply correspond to a "single" infinite string.

The definition of C_n is as follows. The rate at which energy E is radiated by the long strings as gravitational waves in the frequency range $\omega\in(\omega_n,\omega_{n+1})$ in volume V is

$$\text{Power}=\frac{dE_n}{dt}=\frac{V}{t^3}G\mu^2 c C_n\ . \tag{7.2}$$

The volume V is assumed to be changing in time so that $V/a^3(t)$ is a constant; in other words the volume V is the volume of a fixed region in the space $\mathbf{x}$ of the comoving coordinates. To apply this formula to our simulation, we use as the volume the entire simulation box: $V=L_{\rm box}^3 a^3(t)$.

The C_n can now be determined numerically in terms of the corresponding P_n of the infinite strings. We let the index k label the M different infinite strings in the numerical simulation, so $k=1,\ldots,M$. The physical length of the kth string is denoted by L_k, and the gravitational radiation coefficients for the mth mode of the kth string are denoted $P_m^{(k)}$. [These coefficients are defined by Eq. (4.8) where the subscript m denotes the mth mode whose frequency is $4\pi m/L_k$.] One then has

$$C_n=\frac{t^3}{L_{\rm box}^3 a^3(t)}\sum_{k=1}^{M}\sum_{j=0}^{L_k/L_h}P_{j+nL_k/L_h}^{(k)}\ . \tag{7.3}$$

This formula includes in the nth mode C_n the contributions of the L_k/L_h modes of the kth string that lie in the frequency range from ω_n to ω_{n+1}. These L_k/L_h modes are labeled by the index j.

The surprising behavior observed is that the maximum emission from the long strings appears to take place at a *fixed physical frequency* which does not decrease as the horizon length increases. This can be easily seen by examining the graph of the C_n shown in Fig. 7. The graph shows data obtained at three different times, as described in the figure caption. The frequency of maximum emission is given by

$$\omega_{\rm max}\approx 4\pi\frac{8}{L_f}\ , \tag{7.4}$$

where L_f is the horizon length at the time that the string network formed. The wavelength corresponding to this maximum frequency is $\lambda_{\rm max}\approx L_f/16$, which is exactly

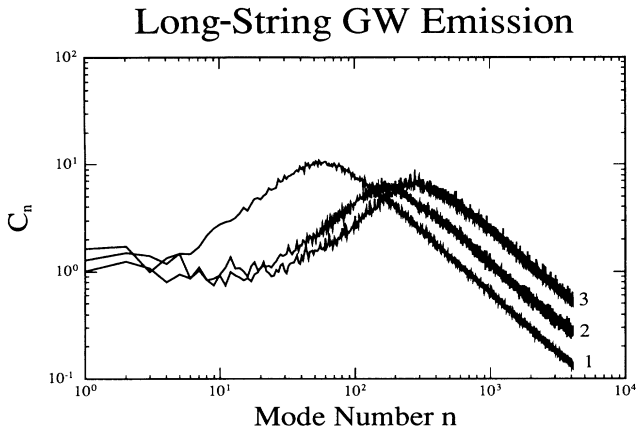

FIG. 7. The energy radiated by the long strings in the form of gravitational radiation is characterized by a set of dimensionless constants C_n, with mode index n corresponding to frequency $4\pi n/L(t)$. Here $L(t)$ is the horizon length. The data for these three curves were taken at different times. For large n, the C_n fall off as $\propto n^{-1.1}$. This was used to estimate the contributions to Γ from large values of n. Curve 1 has $L/L_f=7.65$, $n_{\max}=59$, and $\Gamma=7.7\times10^3$. Curve 2 has $L/L_f=21.0$, $n_{\max}=160$, and $\Gamma=1.3\times10^4$. Curve 3 has $L/L_f=34.2$, $n_{\max}=268$, and $\Gamma=2.3\times10^4$. The characteristic frequency of emission, at which the C_n are peaked, remains constant in time. The C_n are only expected to approach constant values at very late times, when $\Gamma\approx1/(100G\mu)$.

half the correlation length of the string network at its time of formation.

A "true scaling solution" is the term we will use to describe a cosmic-string network for which *every* characteristic length scale increases in proportion to the horizon length $L_h=2t$. For a true scaling solution, the statistical appearance of the string network at time t is identical to that of an earlier time t' after magnification by the dimensionless ratio t/t'. For a true scaling solution, each C_n is a constant, which is independent of time, and thus $\Gamma=\sum_n C_n$ is also independent of time. The rate of energy loss per unit volume into gravitational waves is then

$$\frac{1}{V}\frac{dE}{dt}=t^{-3}G\mu^2\sum_n C_n=t^{-3}G\mu^2\Gamma\ . \tag{7.5}$$

This has the same time dependence as $d\rho_\infty/dt$, where $\rho_\infty=A\mu t^{-2}$ is the energy density in the infinite-string network.

However it can be seen from our graphs that, during the duration of our simulation, the cosmic-string network is not a true scaling solution: the C_n are not constant in time. The reason why can be easily seen if we plot the $C_n(t)$ not as a function of n but instead as a function of physical frequency ω, which is related to n by $\omega=4\pi n/L_h$ giving $n(\omega)=L_h\omega/4\pi$. In Fig. 8, we plot $C_{n(\omega)}$ as a function of the physical frequency ω. One can see immediately that after a period of adjustment (relaxation) the function $C_{\omega t/2\pi}(t)$ appears to become almost *independent* of time t. It is easy to see that this implies that Γ increases linearly with time: the number of modes dn in the frequency interval $d\omega$ is $dn=t\,d\omega/2\pi$, and thus

$$\Gamma=\sum_n C_n=\int C_{n(\omega)}(t)\frac{dn(\omega)}{d\omega}d\omega$$
$$=t/2\pi\int C_{n(\omega)}(t)d\omega\ . \tag{7.6}$$

The value of the final integral, as can be seen from Figs. 8(a) and 8(b), varies only slowly with time once the horizon has expanded by a factor of about 20 from its initial size. This is shown more clearly in Fig. 9, where the data has been smoothed with a 30-point bandwidth. Modeling the results as a power law, one finds that

$$\Gamma\approx Q\left[\frac{t}{t_f}\right]^\kappa \tag{7.7}$$

with $\kappa=0.8\pm0.5$. The actual value of Q depends strongly upon the resolution of the simulation (the number of

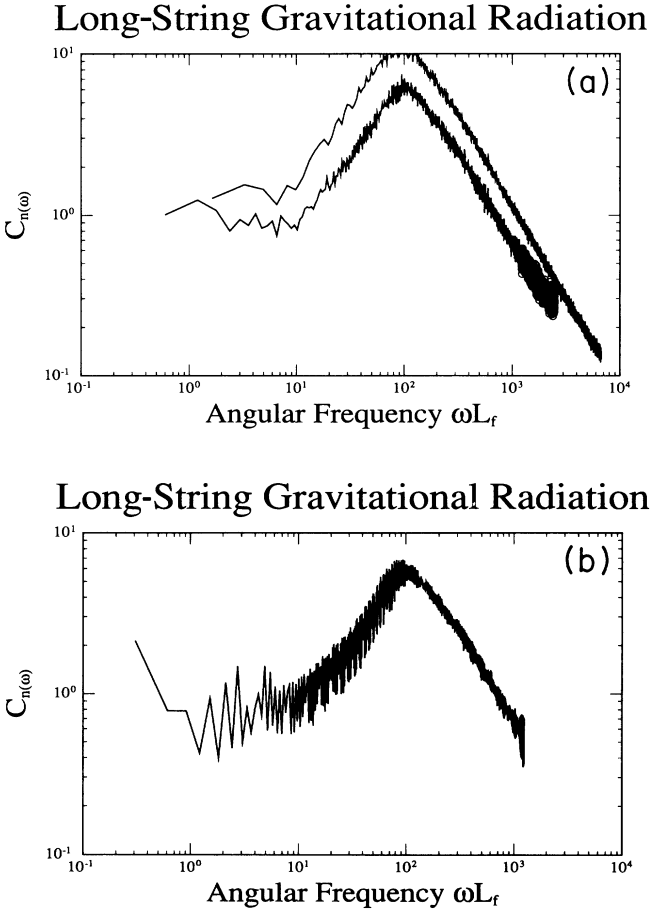

FIG. 8. The C_n are shown as a function of the physical frequency ω. After an initial period of relaxation, the function $C_{n(\omega)}$ becomes constant in time. They are peaked about $\omega L_f\approx10^2$, where the wavelength is half the correlation length of the long-string network at the time of formation. (a) The $C_{n(\omega)}$ are shown at two times, $L/L_f=7.65$ (upper curve) and $L/L_f=21.0$ (lower curve). (b) The $C_{n(\omega)}$ are now shown at a later time; $L/L_f=40.2$, where they have not changed significantly from earlier times. If this curve does not change with time, then since the number of modes in any given frequency interval $d\omega$ increases linearly with time, Γ increases linearly with time.

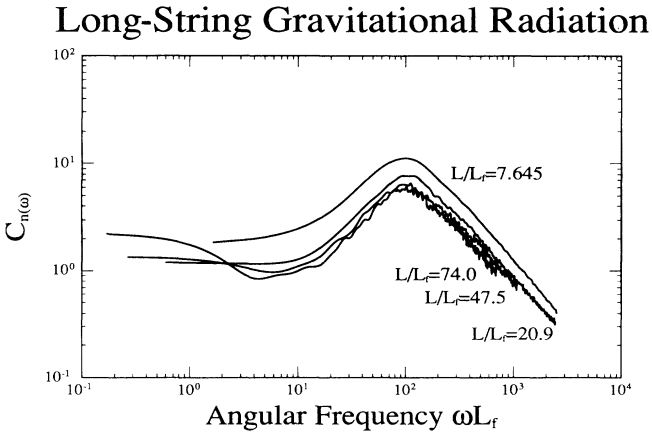

FIG. 9. This graph shows the gravitational-radiation coefficients $C(t)_{n(\omega)}$ as a function of physical angular frequency ω at four different times. The values of L/L_f show the ratio of the current horizon scale to the horizon scale at the time that the string network was formed. The $C(t)_{n(\omega)}$ cease to depend upon t at late times, and are only a function of ω. While they do decrease slightly with time, this decrease is much less rapid than $1/t$ and implies that the energy radiated per unit length of long string is approximately constant in time. The data in these graphs has been smoothed with a bandwidth of 30 points, to prevent the scatter in the graphs from smearing the graphs together.

string points per initial correlation length divided by the minimum number of points in a loop). As might be expected, when the resolution is low (of order $\frac{3}{2}$), it is difficult for the long strings to shed their small-scale structure, and $Q \approx 750$. For high-resolution (of order 4) runs the long strings lose much of their small-scale structure and $Q \approx 100$ is considerably smaller. Part of this decrease in Q is due to a decrease in the long-string energy density associated with the higher resolution, but the majority of the change is due to the reduction in small-scale structure on the long strings. However the fact remains that in both the high- and low-resolution runs, the peak of the C_n is at a *fixed* physical frequency, and Γ grows with time. This increase in Γ appears to be due to the presence of persistent structure on the cosmic-string network at a fixed physical length scale equal to the initial correlation length of the string network. The presence of this structure is not entirely surprising; it is predicted by recent analytic work showing that structures approach a constant mean separation of order t_f [7,8,9]. In this case, however, the structures appear to be more closely related to the initial conditions of the string network, which is formed with perturbations of length t_f. These perturbations persist even at late times.

Other research has investigated the small-scale structure on the long strings, primarily through the use of the fractal dimension, which measures the "straightness" of the string on a given length scale. That work showed that, as time goes by, the strings always straighten out on a fixed physical length scale [5,6]. Our results appear somewhat different. At early times, the emission of gravitational waves at a fixed physical frequency decreases; however after about 20 expansion times the emission at a fixed physical frequency is only slowly decreasing—certainly less quickly than $1/t$. Our results seem to show that once the amplitude of the small-wavelength perturbations on the strings becomes small enough, the expansion of the universe does not strongly damp the oscillations. These small-amplitude perturbations at small wavelengths do not show up as clearly in the fractal curves used previously to analyze the small-scale structure on the long strings. This is due, in part, to the shorter lifetimes of high-frequency modes; they radiate away their energy more quickly and dominate the spectrum of gravity waves (especially when back reaction is not included).

Because the numerical simulations can only run for a limited amount of time, it is impossible to follow the increase in Γ for a long period in time. It is therefore necessary to extrapolate the observed increase, and to speculate about the physical effects that prevent Γ from increasing indefinitely. Eventually, one expects Γ to become large enough so that the rate of energy loss into gravitational waves becomes comparable to the rate of energy loss into the formation of loops. This occurs when $V^{-1}d(VA\mu t^{-2})/dt \approx \Gamma G\mu^2 t^{-3}$ which implies $\Gamma \approx A/2G\mu$. This occurs when t/t_f lies in the range $10^{-2}/G\mu$ to $10^{-1}/G\mu$. After this time, our expectation is that the C_n will indeed become constant in time, with $\Gamma \approx A/2G\mu$. In the following, we shall assume for the purposes of discussion that Γ increases linearly, $\kappa \approx 1$ in (7.7).

VIII. CONCLUSIONS

In this section, we compare the different ways in which the infinite-string network converts its energy into gravitational radiation. This conversion of energy is effected via two mechanisms: (1) the direct emission of gravitational radiation by the long strings, as considered in the previous section; (2) the production of loops which subsequently convert their energy into gravitational radiation.

The rate at which the infinite string loses energy into gravitational waves is determined by $\Gamma = \sum_n C_n$. In a fixed comoving volume V of the universe, in time dt the infinite strings lose an amount of energy

$$dE^{\infty}_{\text{grav wave}} = dt\, Vt^{-3} G\mu^2 c\Gamma \ . \tag{8.1}$$

(Note: from this point on, we use the superscript on E to denote the type of string losing energy, and the subscript on E to indicate by which mechanism the energy is lost.) It is straightforward to compare this rate of energy loss to the other means by which the long strings lose energy: the formation of loops. The energy density in the infinite strings is $\rho_\infty = A\mu t^{-2}$ with $A \approx 16$. Hence, in time dt the infinite-string network loses an amount of energy into loop formation and stretching given by

$$dE^{\infty}_{\text{loop form}} = \tfrac{1}{2} dt\, Vt^{-3} A\mu \ . \tag{8.2}$$

If the mean velocity squared of the infinite-string network were $\frac{1}{2}$ then there would be no stretching, and all the energy would be lost to loop formation. Since $\langle v^2 \rangle \approx 0.43$

this is a reasonable approximation to make, and we make it. The ratio of the two energy-loss rates is then

$$\frac{\dot{E}^{\infty}_{\text{grav wave}}}{\dot{E}^{\infty}_{\text{loop form}}} = \frac{2G\mu\Gamma}{A} . \tag{8.3}$$

Our expectation, as explained in the previous section, is that Γ will increase until the right-hand side of Eq. (8.3) is of order one, after which time Γ will remain constant. In this case, the two energy-loss mechanisms are very roughly comparable in magnitude: $\dot{E}^{\infty}_{\text{grav wave}} \sim \dot{E}^{\infty}_{\text{loop form}}$. If some other effect intervenes, and prevents Γ from reaching this large value, perhaps, because we have underestimated the smoothing effect of gravitational back reaction, then we would have $\dot{E}^{\infty}_{\text{grav wave}} < \dot{E}^{\infty}_{\text{loop form}}$.

It is also possible to compare these energy-loss rates with the rate at which gravitational radiation is emitted by the loops of string. To do this, we make the standard assumptions of the one-scale model. A loop formed at time t' is assumed to have a length $\alpha t'$. (The numerical simulations have not clearly established the size of the dimensionless parameter α, but have shown that $\alpha < 10^{-2}$.) Hence the power emitted by all surviving loops in the form of gravitational radiation at time t is given by

$$\begin{aligned}\dot{E}^{\text{loops}}_{\text{grav wave}} &= \int_{\beta t}^{t} dt' \frac{dN}{dt'} \gamma G\mu^2 \\ &= \tfrac{1}{3} V t^{-3} A \alpha^{-1} \gamma G\mu^2 (\beta^{-3/2} - 1) .\end{aligned} \tag{8.4}$$

Here $dN/dt = \frac{1}{2} A \alpha^{-1} V t^{-4}$ is the rate of loop formation in the volume V, and $\beta = \gamma G\mu/(\alpha + \gamma G\mu)$ determines the lifetime of the loops.

There are two possibilities, depending upon the relative magnitudes of α and $\gamma G\mu$. The most likely possibility is that $\alpha > \gamma G\mu$, in which case

$$E^{\text{loops}}_{\text{grav wave}} = \tfrac{1}{3} dt\ V t^{-3} A\mu \frac{\alpha^{1/2}}{(\gamma G\mu)^{1/2}} . \tag{8.5}$$

In this case, the relative magnitudes of these three energy-loss mechanisms are

$$\dot{E}^{\infty}_{\text{grav wave}} \sim \dot{E}^{\infty}_{\text{loop form}} < \dot{E}^{\text{loops}}_{\text{grav wave}} . \tag{8.6}$$

The other possibility, which we consider less likely, is that the loops are chopped off the string network at a length scale α *smaller* than $\gamma G\mu$. In this case, one has $\beta \approx 1 + \alpha/(\gamma G\mu)$ and hence

$$E_{\text{grav wave}} = \tfrac{1}{2} dt\ V t^{-3} A\mu . \tag{8.7}$$

In this case, the loops which are formed are so small that they radiate away their energy almost instantly, and so the rate at which the infinite strings transfer energy into loops is the same as the rate at which the loops convert their energy into gravitational radiation. In this case, one has

$$\dot{E}^{\infty}_{\text{grav wave}} \sim \dot{E}^{\infty}_{\text{loop form}} \sim \dot{E}^{\text{loops}}_{\text{grav wave}} . \tag{8.8}$$

However, in either case, it appears that while the power radiated in gravitational radiation by long strings is a significant energy-decay mechanism, it will never exceed the power radiated in gravitational radiation by the loops of string.

There are three observational constraints on the gravitational perturbations produced by cosmic strings, arising from the standard model of nucleosynthesis, the timing noise in pulsars, and the isotropy of the microwave background radiation. The results of this work have some bearing on the first two of these constraints. This issue is investigated in more detail in work currently in progress [18].

ACKNOWLEDGMENTS

We would like to acknowledge useful discussions with D. Bennett, F. Bouchet, R. Caldwell, T. Vachaspati, and A. Vilenkin. This work has been partially supported by NSF Grants Nos. 87-05107, 89-03027, and 91-05935 (B.A.) and by SERC and Trinity College, Cambridge (E.P.S.S.).

[1] T. W. B. Kibble, J. Phys. A **9**, 1387 (1976); T. W. B. Kibble, G. Lazarides, and Q. Shafi, Phys. Rev. D **26**, 435 (1982); T. W. B. Kibble and N. Turok, Phys. Lett. **116B**, 141 (1982); T. W. B. Kibble, Nucl. Phys. **B252**, 227 (1985); T. W. B. Kibble and E. Copeland, Imperial College Report No. TP/89-90/27, 1990 (unpublished).

[2] Y. B. Zel'dovich, Mon. Not. R. Astron. Soc. **192**, 663 (1980).

[3] A. Vilenkin, Phys. Rev. Lett. **46**, 1169 (1981); **46**, 1496(E) (1981); Phys. Rev. D **24**, 2082 (1981); A. Vilenkin and J. Silk, Phys. Rev. Lett. **53**, 1700 (1984); A. Vilenkin, Phys. Rep. **121**, 263 (1985); Nature (London) **343**, 591 (1990).

[4] A. Albrecht and N. Turok, Phys. Rev. Lett. **54**, 1868 (1985); Phys. Rev. D **40**, 973 (1989); A. Albrecht, in *The Formation and Evolution of Cosmic Strings,* Proceedings of the Symposium, Cambridge, England, 1989, edited by G. W. Gibbons, S. W. Hawking, and T. Vachaspati (Cambridge University Press, Cambridge, England, 1989); N. Turok, *ibid.*

[5] D. Bennett and F. Bouchet, Phys. Rev. Lett. **60**, 257 (1988); **63**, 2776 (1989); Astrophys. J. **354**, L41 (1990); in *The Formation and Evolution of Cosmic Strings* [4]; Phys. Rev. D **41**, 2408 (1990).

[6] B. Allen and E. P. S. Shellard, Phys. Rev. Lett. **64**, 119 (1990); E. P. S. Shellard and B. Allen, in *The Formation and Evolution of Cosmic Strings* [4].

[7] B. Allen and R. R. Caldwell, Phys. Rev. Lett. **65**, 1705 (1990); in *Proceedings of the Banff Summer School on Gravitation, 1990,* edited by R. Mann (World Scientific, New York, 1991), p. 65; in *Nonlinear Problems in Relativity and Cosmology,* Proceedings of the Conference on Nonlinear Physics, Gainesville, Florida, 1990, edited by J. R. Buchler, S. L. Detweiler, and J. R. Ipser [Ann. N.Y. Acad. Sci. **631**, 76 (1991)]; Phys. Rev. D **43**, 2457 (1991); **43**, 3173 (1991).

[8] J. M. Quashnock and T. Piran, Phys. Rev. D **43**, 3785 (1991).

[9] M. Hindmarsh, Phys. Lett. B **251**, 28 (1990).

[10] A. Vilenkin, Phys. Lett. **107B**, 47 (1981).

[11] N. Turok, Nucl. Phys. **B242**, 520 (1984).

[12] T. Vachaspati and A. Vilenkin, Phys. Rev. D **31**, 3052 (1985).
[13] C. Burden, Phys. Lett. **164B**, 277 (1985).
[14] D. Garfinkle and T. Vachaspati, Phys. Rev. D **36**, 2229 (1987); **37**, 257 (1988).
[15] R. J. Scherrer, J. M. Quashnock, D. N. Spergel, and W. H. Press, Phys. Rev. D **42**, 1908 (1990).
[16] J. M. Quashnock and D. N. Spergel, Phys. Rev. D **42**, 2505 (1990).
[17] S. Weinberg, *Gravitation and Cosmology* (Wiley, New York, 1972).
[18] R. R. Caldwell and B. Allen, Phys. Rev. D (to be published).

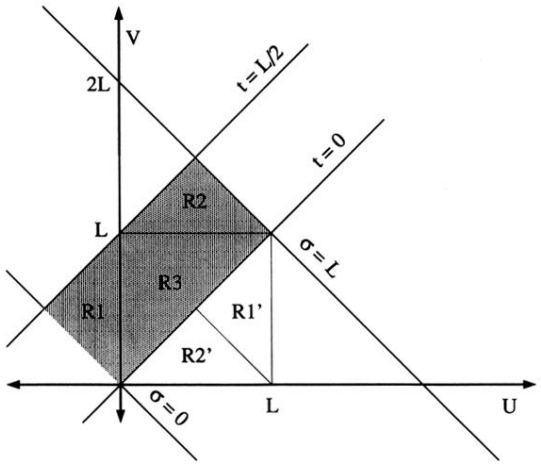

FIG. 1. The region over the (u,v) plane used to evaluate the integral in Eq. (3.16). The integrand (3.15) is the same in regions $R1$ and $R1'$ and in regions $R2$ and $R2'$. Hence the integral over the shaded region equals the integral over the $L \times L$ square.